Journal of the American Ceramic Society

Structure-mechanical properties correlation in bulk LiPON glass produced by nitridation of metaphosphate melts

V. M. Torres III[1], S. Kalnaus[2*], S. W. Martin[1*], C. Duggan[3], A. S. Westover[4]

[1] Department of Materials Science and Engineering, Iowa State University, Ames, IA 50011, USA
[2] Computational Sciences and Engineering Division, Oak Ridge National Laboratory, Oak Ridge, TN 37831, USA
[3] Materials Science and Technology Division, Oak Ridge National Laboratory, Oak Ridge, TN 37831, USA
[4] Chemical Sciences Division, Oak Ridge National Laboratory, Oak Ridge, TN 37831, USA

Abstract
The glassy solid electrolyte Lithium phosphorous oxynitride (LiPON) has been widely researched in thin film solid state battery format due to its outstanding stability when cycled against lithium. In addition, recent reports show thin film LiPON having interesting mechanical behaviors, especially its ability to resist micro-scale cracking via densification and shear flow. In the present study, we have produced bulk LiPON glasses with varying nitrogen contents by ammonolysis of $LiPO_3$ melts. The resulting compositions were determined to be $LiPO_{3-3z/2}N_z$, where $0 \leq z \leq 0.75$, and the z value of 0.75 is among the highest ever reported for this series of LiPON glasses. The short-range order structures of the different resulting compositions were characterized by infrared, Raman, ^{31}P magic angle spinning nuclear magnetic resonance, and x-ray photoelectron spectroscopies. Instrumented nano-indentation was used to measure mechanical properties. It was observed that similar to previous studies, both trigonally coordinated (N_t) and doubly bonded (N_d) N co-exist in the glasses in about the same amounts for $z \leq 0.36$, the limit of N content in most previous studies. For glasses with $z > 0.36$, it was found that the fraction of the N_t increased significantly while the fraction of N_d correspondingly decreased. The incorporation of nitrogen increased both the elastic modulus and hardness of the glass by approximately a factor of 1.5 when N/P ratio reaches 0.75. At the same time, an apparent embrittlement of the glass was observed due to nitridation which was revealed by nanoindentation with an extra sharp nanoindenter tip.

Keywords: Glass, Solid State Battery, Electrolyte, Mechanics

*Corresponding authors. Email: kalnauss@ornl.gov (S. Kalnaus); swmartin@iastate.edu (S.W. Martin)

NOTICE OF COPYRIGHT

Notice: This manuscript has been authored by UT-Battelle LLC under contract DE-AC05-00OR22725 with the US Department of Energy (DOE). The US government retains and the publisher, by accepting the article for publication, acknowledges that the US government retains a nonexclusive, paid-up, irrevocable, worldwide license to publish or reproduce the published form of this manuscript, or allow others to do so, for US government purposes. DOE will provide public access to these results of federally sponsored research in accordance with the DOE Public Access Plan (http://energy.gov/downloads/doe-public-access-plan).

1. Introduction

Solid state lithium metal batteries promise a dramatic increase in energy density combined with improved safety compared with the traditional liquid electrolyte-based batteries.[1, 2] While the potential benefits are obvious, the solid-state battery, apart from thin-film format, so far remains in the conceptualization stage due to numerous problems that need to be solved in materials science, physics, and engineering aspects before successful commercialization can be achieved.[3] The critical component of a high energy density solid state battery cell is the solid electrolyte (SE) which needs to maintain robust interfaces with both cathode and metallic lithium anode while preventing any electronic current between the electrodes over many cycles of charge and discharge. In addition, it needs to have high ionic conductivity and robust chemical stability with electrode materials (typically layered transition metal oxides as a positive electrode and lithium as a negative electrode). Further, it is obvious that the list of requirements for a robust SE combines these chemical and electrochemical properties with suitable mechanical behavior. While a significant amount of research has been focused on the ionic conductivity, with values approaching 10^{-2} S/cm in $Li_{10}GeP_2S_{12}$,[4] for example, the mechanical behavior of SEs, apart from their elastic properties, has been for the most part overlooked. The mechanics of SEs is important in several aspects: i) the SE should enable uniform plating and stripping of lithium and prevent the formation and penetration of lithium filaments (often termed "dendrites" in the battery community); ii) it should maintain intimate contact with the anode and cathode while allowing for compositional strains accompanying volume expansion and contraction during charge and discharge cycles and ; iii) ideally, it should be processable at low cost, at scale, in bulk, and suitable for high volume roll-to-roll manufacturing.

Currently, there are very few, if any ion conducting glass, ceramic, or glass ceramic SEs that satisfy all three of the above criteria. Most polycrystalline ceramic SEs fail due to lithium dendrite growth and penetration, which proceeds either transgranularly or intergranulary, when cycled in cells at useable current densities.[5] This has been attributed to low fracture toughness of ceramic ion conductors (typically less than 1 MPa $m^{1/2}$) combined with reduced bandgap at the grain boundaries which leads to the leakage electronic current and lithium plating along the grain boundaries.[6-9] Glassy SE (GSE) ionic conductors would eliminate the issue connected with the grain boundaries. Among various GSEs, lithium phosphorous oxynitride (LiPON) glass has been demonstrated to electrochemically cycle lithium over thousands of cycles without forming lithium

penetrating dendrites.[10] The ability of LiPON to prevent lithium penetration is connected to its rather interesting mechanical properties; it demonstrates extremely high resistance to nanoindentation fracture by relieving applied stress via a combination of shear flow and densification.[11-13] Such performance however has only been demonstrated in thin-film (~ 1-5 μm) formats, where LiPON is deposited via radio frequency (RF) magnetron sputtering of Li_3PO_4 target. On the one hand this presents a major limitation to producing required films that are typically 10s of μm at low cost, but on the other hand it allows producing glass films with very high Li content (Li:P ~ 3).

However, in a very different nitridation process, nitrogen can be introduced into bulk phosphate glasses by a process where oxygen is replaced by nitrogen during anerobic ammonia flow over a molten base metaphosphate glass, $LiPO_3$, at temperatures typically below the thermal decomposition temperature of NH_3.[14] In these oxynitride glasses the lithium content is three times lower (Li:P = 1) than in thin-film LiPONs resulting from the sputtering of Li_3PO_4. The structure of $LiPO_3$ glass is comprised of lithium cations (Li^+) and P^2 phosphate anions, where the subscript refers to the number of bridging oxygens of the form $PO(O)O_2O^{-1}$ or PO_3^{-1} which are arranged in a random long chain disordered network. The chains have been estimated to be on the order of 1,000 or so repeat units in length, terminating at the end by P^1 end units. These P^2 phosphate anions are in the form of tetrahedral units, with two oxygen atoms bonded to two phosphorus atoms, one oxygen doubly bonded to the P and one oxygen covalently bonded to P and one bonded ionically to one lithium cation. The lithium cations are tetrahedrally coordinated by oxygen atoms. LiPON is a network of interconnected tetrahedra composed of a central phosphorus atom surrounded by four oxygen or nitrogen atoms. Nitrogen exists in two coordinations, either as a doubly bonded nitrogen N_d, P-N=P and a trigonally bonded form N_t, $P-N<^{P}_{P}$. Recently, we applied ammonolysis to $LiPO_3$ and $NaPO_3$ base melts and obtained LiPON and NaPON oxynitride glasses[15] in bulk form. In the current report, we utilize this same procedure to obtain a series of bulk LiPON GSEs of general composition $LiPO_{3-3z/2}N_z$, where $0 \leq z \leq 0.75$, with different nitrogen contents, ranging from N/P = 0 to N/P = 0.75. We characterized the resulting glasses using IR, Raman, ^{31}P magic angle spinning nuclear magnetic resonance (MAS NMR), and x-ray photoelectron (XPS) spectroscopies to obtain detailed short range order (SRO) structural information about these LiPON GSEs. Finally, we correlate the SRO structures of these GSEs with their mechanical properties determined by instrumented nanoindentation. Substantial increase in both hardness and

elastic modulus was observed with an increase of nitrogen content (z) in these LiPON GSE compositions. In addition, high-nitrogen glasses, z > 0.36, showed substantial increase in brittleness.

2. Experiment

2.1. Metaphosphate base glass preparation

Lithium metaphosphate, $LiPO_3$, was synthesized from stoichiometric amounts of Li_2CO_3 (Alfa Aesar 99%) and $(NH_4)_2HPO_4$ (Acros 99+%) to produce the $50Li_2O + 50P_2O_5$ composition. These compounds were mixed with a large mortar and pestle, transferred to a porcelain crucible, and placed into a furnace. The crucible was then heated at 1°C/min from 25°C to 200°C, held for 4 hours, heated to 600°C, held for 4 hours to promote the removal of NH_3, CO_2, and H_2O, heated to 800°C and held for at least 2 hours. Approximately from the 100 grams of starting materials, 22 grams of LiPO3 is obtained in the porcelain crucible. To synthesize the LiPON needed, 2 separate batches of Li2CO3 and NH42HPO4 were massed, mixed, and melted on separate days. However, these materials were massed out to equal, and nearly identical amounts and followed the same identical heating profile. These materials were cast into bars 1 cm by 4 cm with a thickness of ~1 cm. The melt was then quenched to room temperature onto a brass mold and stored in a glovebox to keep the $LiPO_3$ dry from H_2O.

2.2. Ammonolysis of $LiPO_3$

Bulk samples of LiPON glass were synthesized from the $LiPO_3$ prepared above by using the method by De Souza *et al.* [15] A bulk sample of $LiPO_3$, ~5 g, glass was nitrided through ammonolysis using gaseous NH_3 for various hold times ranging from 0.5 to 7 hours at 750°C inside of a vitreous carbon crucible boat. The reaction between $LiPO_3$ and NH_3 is given in Eq. (1) shown below.

$$LiPO_3 + zNH_3 \rightarrow LiPO_{3-3z/2}N_z + 3z/2H_2O \qquad \text{Eq. (1)}$$

The weight loss of the $LiPO_3$ glass due to exchange of 3 atoms of Oxygen for 2 atoms of Nitrogen from the melt was determined by measuring the mass of the sample before (m_b) and after

ammonolysis (m_a). Utilizing the method of De Souza *et al.* [15] the nitrogen to phosphorous ratio (z = N/P) was determined for each sample using Eq. (2).

$$N/P = z = (85.884)(m_b-m_a)/9.992 \quad \text{Eq. (2)}$$

In Eq. (2) 85.884 g/mol is the formula weight of $LiPO_3$, (m_b-m_a) is the mass loss due to ammonolysis, which is assumed to be H_2O according to Eq. (1), and 9.992 g/mol is the oxygen to nitrogen weight exchange ratio. The N/P ratio was used to determine the specific composition of $LiPO_{3-3z/2}N_z$ using Eq. (2). Over the 0 to 6 hour time range of ammonolysis used here, it was found that $0 \leq z \leq 0.75$.

2.3.Nanoindentation

Instrumented nanoindentation was performed using the InForce 1000 actuator by Nanomechanics Inc., a KLA company. The actuator has a maximum load of 1N and 6 nN load resolution. The actuator with a frame was installed inside the Tescan Mira 3 Scanning Electron Microscope (SEM) which allowed for a small-angle in-situ monitoring of the nanoindentation process. The same SEM was used to examine the residual hardness impressions after nanoindentation. Elastic modulus and hardness were measured using a Berkovich nanoindenter tip with the central angle of 65.03°. For each sample, nanoindentation was performed at two random locations on the sample surface. Each location contained a 5x5 matrix of nanoindentations with 30 μm spacing between the adjacent nanoindentations. Thus 50 nanoindentation curves were collected per each sample. A standard calibration procedure was applied before each set of tests.[16] The tip area function and frame stiffness were calibrated using a fused silica sample, - a standard choice of material due to its well-known properties and absence of pile-up during nanoindentation. The polynomial tip area function was calibrated using the data from 16 nanoindentations and the calibrated parameters yielded the Young's modulus of fused silica equal to 73.5 Gpa, which is very close to the reported values.[16] In the above procedure, the Poisson's ratio of fused silica was taken as 0.188.

The pieces of glass produced by ammonolysis were cold mounted in epoxy (Buehler). Grinding was done with 1200 grit sandpaper to expose the surface for polishing. Subsequent polishing was performed using oil-based diamond suspensions with decreasing particle size from

6 μm to 1 μm. The final polishing step was performed on a Saphir Vibro polishing bowl using the MD-DUR (Struers) polishing cloth and fumed silica. Rinsing between the steps was done with acetone. The procedure was carefully designed to get a nanoindentation ready specimen surface without any exposure of samples to water. The polished glass cast in epoxy was attached to an aluminum stub for nanoindentation and SEM analysis using permanent glue.

Measurements of mechanical properties, Young's modulus and hardness, were performed using the Berkovich nanoindenter tip in continuous stiffness measurement (CSM) mode. In this mode, small amplitude (2nm) high frequency (100 Hz) oscillations are applied to the tip as it is driven into the material which allows the mechanical properties to be probed as a function of depth. The loading was done in target strain rate of 0.2 1/s. Thermal drift was measured at the beginning of each experiment with the target value of less than 0.1 nm/s. The drift was also measured using the 80 s hold under one-tenth of the peak load at the end of each nanoindentation loading within the matrix. Resistance to fracture in glass was probed by nanoindentation with a sharp cube corner nanoindenter tip (central angle of 35.26^{o}). This test creates a high intensity stress under the nanoindenter tip thus reducing the threshold load for fracture.[17] All tests were done at room temperature and under SEM vacuum.

2.4 Spectroscopic and nitrogen content analysis

2.4.1 Raman Spectroscopy

The Raman spectra were collected using an XploRA Plus Raman confocal upright microscope (HORIBA Scientific, Edison, NJ) with a Synapse EMCCD camera, equipped with a 532 nm solid state diode laser operating at 11.67 mW. The Raman spectra were collected by scanning over a spectral range of 100 cm^{-1} to 1700 cm^{-1} using an acquisition time of 10 seconds with a maximum of 15 accumulations. Samples were measured twice, in two different locations, to examine if the spectra changed over the surface of the glass sample. No sample heating or fluorescence was observed in the spectra.

2.4.2 Fourier Transformation Infrared (FT-IR) Spectroscopy

Samples were prepared for FT-IR measurements by diluting the glass samples with cesium iodide (CsI) in a mass ratio of 1:40. The materials were ground into a fine powder with a mortar and pestle and pressed into a thin, ~100 μm to 200 μm, pellet inside a N_2 glovebox. Samples were

transferred to a Bruker IFS 66v/s FT-IR spectrometer where 32 scans from 400 cm^{-1} to 1600 cm^{-1} at 4 cm^{-1} resolution were collected for each sample.

2.4.3 ^{31}P Magic Angle Spinning Nuclear Magnetic Resonance (MAS NMR) Spectroscopy

^{31}P MAS NMR spectra were collected using a 400 MHz Bruker Avance spectrometer using 4 mm zirconia rotors spun at 12.5 kHz. The samples were ground into a fine powder inside a N_2 glovebox and tightly sealed to retain an inert atmosphere. H_3PO_4 was used as the chemical shift reference for the ^{31}P MAS NMR spectra. A delay time of 90 seconds between each of 256 scans enabled the spectra to be collected in ~1 hour. The pulse width was 6 μs and the pulse power was 10 dB.

2.4.4 X-ray Photoelectron Spectroscopy (XPS)

The XPS measurements were performed using a Kratos Amicus/ESCA 3400 spectrometer. Spectra were acquired for each of three scans on a single sample with the first scan corresponding to the surface of the sample, and two scans were then collected after a first 300 s and a second 300 s etch from a beam of 500 eV Ar^+ ions applied to the sample. The binding energies of the spectra were normalized to adventitious surface carbon which has a signal at 286.4 eV.

3 Results and discussion

3.1 Structure analysis

The incorporation of nitrogen into the $LiPO_3$ glass network causes structural changes which were examined using Raman, FT-IR, and ^{31}P MAS NMR spectroscopies, and XPS. The Raman spectra of the glasses are shown in Fig. (1A) as a function of the N/P ratio for each glass with the various assignments of the peaks labeled. The assignments on the spectra follow the well-known assignments of these peaks from our[18-21] and others work.[22-24] The increase in peak intensity from 175 cm^{-1} to 400 cm^{-1} corresponds to the bending vibration and deformation modes of the O-P-N bonds in the phosphate glass structure. The Raman active modes corresponding to the symmetric stretches of P-O-P, $P_2O_7^{4-}$ (P^1), O-P-O (P^2) , and P=O short range order (SRO) structures are located at 695, 1022, 1151-1176, and 1355 cm^{-1}, respectively. [15, 25] The superscript in the notation is the number of bridging oxygens (BOs) in the SRO structure. As nitrogen is incorporated into

the glasses, new bands develop which are located at 645 cm^{-1} and 820 cm^{-1} and correspond to the tri-coordinated nitrogen, N_t, $P-N<_P^P$, and the di-coordinated nitrogen, N_d, P-N=P, respectively.[26]

The most intense peak observed in the Raman spectra is as expected[18-21] the symmetric stretch of the O-P-O (P^2) SRO structure at 1151 cm^{-1} to 1176 cm^{-1}, and broadens with the increase in the N/P ratio. From these results, we conclude that the nitrogen enters the glass network and breaks up the (P-O-P) BO unit to form the tri-coordinated nitrogen, $P-N<_P^P$ and the di-coordinated nitrogen, P-N=P species. As such, the incorporation of nitrogen into these glasses leads to the formation of two new $PO_{4-x}N_x$ tetrahedra, $PO_2N_2^{-1}$ and PO_3N^{-1} SRO species,[1] and to the formation of an additional pure oxide SRO species, the $P_2O_7^{4-}$ (P^1) species. The P^1 species has a mode at 1022 cm^{-1}. All of these charged species necessarily form because there must be overall charge compensation of the Li^+ in the glass. The P^1 SRO species, due to it possessing two non-bridging oxygens (NBOs), act as chain terminating species to the metaphosphate chains. The formation of the two charged $PO_2N_2^{-1}$ and PO_3N^{-1} species and more highly charged P^1 SRO species, necessarily causes a strong decrease in the fraction of the original P^2 SRO species. To characterize these glasses further, we next turn to the FT-IR spectra which are more sensitive to these more charged bonded species.

Figure (1B) gives the FT-IR spectra for these LiPON glasses and the P-O modes that are the most intense modes for these glasses. That is, as found by others there are no new definitive modes associated with P-N bonds in these LiPON GSEs. [18-24] The bands present in the FT-IR spectra are significantly broader than those in the Raman spectra and can be observed to remain consistent through each spectra. The peaks in the FT-IR spectra correspond to the δ(O-P-O), ν_{sym} (P-O-P), ν_{asym} (P-O-P), ν_{asym} (PO_3^{1-}), ν_{asym} (PO^{2-}), and ν_{asym} P=O modes and are located in the ranges of 420 to 620 cm^{-1}, 670 to 800 cm^{-1}, 840 to 950 cm^{-1}, 980 to 1020 cm^{-1}, 1090 to 1150 cm^{-1}, and 1240 to 1270 cm^{-1} respectively.[27-29] As seen, the P-O-P bonds corresponding to the metaphosphate chain structures are observed to decrease in intensity as nitrogen incorporation increases. This is to be expected as the N_t and N_d species replace the P-O-P bonds in the $LiPO_3$ glass structure.

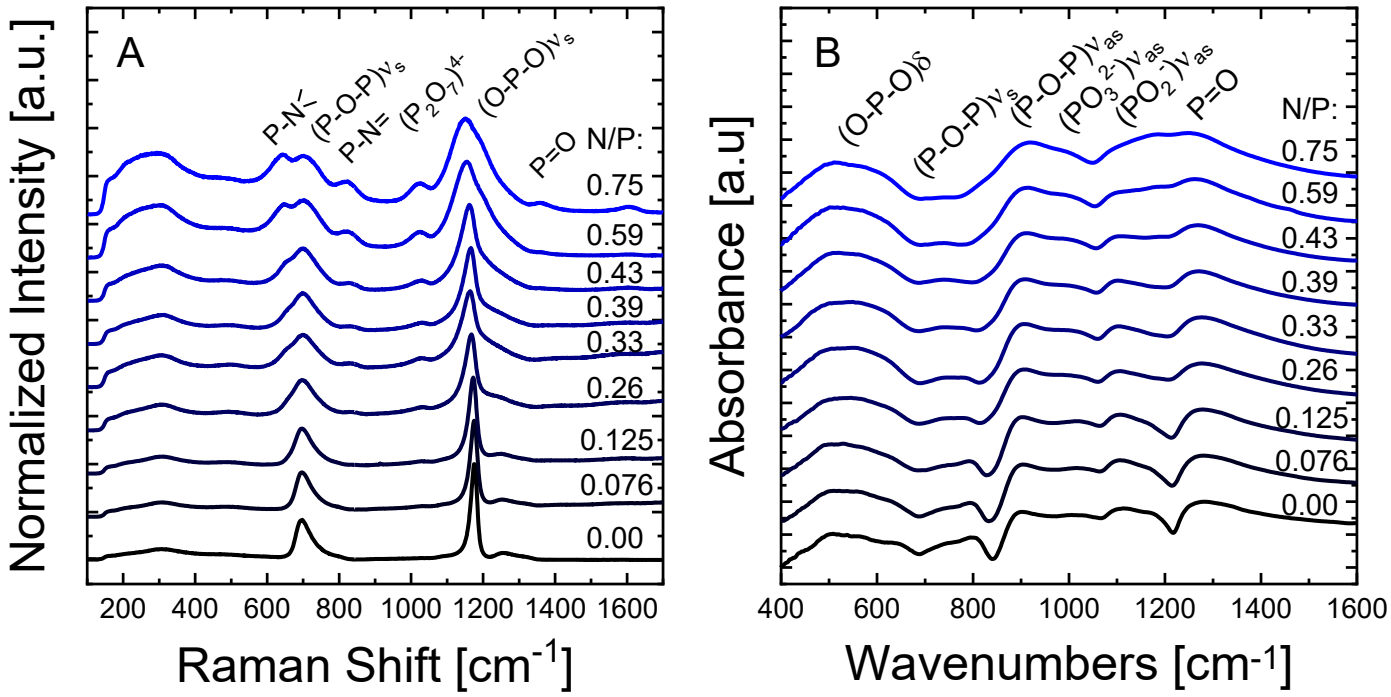

Figure 1. Raman (A) and FT-IR spectra (B) of LiPON GSEs with increasing amounts of nitrogen incorporation into the glasses. Peaks are identified on each of the spectra and changes can be observed in each with increasing incorporation of nitrogen.

In addition to the Raman and FT-IR spectra, the Li1s, P2p, N1s, and O1s XPS spectra were collected for these glasses, Fig. 2. For the Li1s spectra, there is only one observable emission peak and it is located at 55.5 eV and remains relatively constant across all compositions as the N content increases.[30] The P2p XPS peak is composed of the two closely spaced spin-orbit components. The P $2P_{3/2}$ component is located at 134.1 to 133.8 eV, and the P $2P_{1/2}$ is located at 134.7 to134.4 eV. The binding energies of both components remain relatively unchanged with N/P ratio.[31] The N1s spectra shows two peaks at 399.1 eV and 397.5 eV corresponding to the N_t, $P-N<^{P}_{P}$, and the N_d, P-N=P, species respectively.[32] It is important to point out that there is a very small, but none-the-less statistically significant N1s signal for the nominally N-free glass $LiPO_3$. This minor signal comes from the presence of NH_3 gas as a decomposition product, Eq. (3), of the ammoniated starting materials used to make the $LiPO_3$, $(NH_4)_2HPO_4$. Here, the by-product $NH_3(g)$ is present as a gas above the $LiPO_3$ melt and can react with the $LiPO_3$ melt in exactly the same way described above as flowing NH_3 gas over the $LiPO_3$ melt during the ammonolysis process.

$$2(NH_4)_2HPO_4 \rightarrow 4NH_3(g) + 3H_2O(g) + P_2O_5(l) \qquad \text{Eq. (3)}$$

Lastly, the O1s spectra shows two main peaks which are assigned to the BO and NBO species, which are located at 533.2 eV and 531.4 eV, respectively. The BO species is comprised of the P-O-P bonds, while the NBO species are comprised of the P=O and P-O^-Li^+ bonds.[33]

The Li1s and O1s spectra remain relatively constant with increasing nitrogen content. The P $2P_{3/2}$ peak is located at 134.1 eV and with increasing N content, this peak shifts to a lower binding energy due largely to the lower electronegativity of the nitrogen which is replacing P-O bonds for P-N bonds. In addition to this change in the P2p XPS spectra, there is a change in relative intensities of the N1s XPS peaks assigned to the N_t and N_d species. Specifically, as more nitrogen is incorporated into the glass, the N_t, which is originally the predominant species, becomes the less predominant species and the N_d becomes the predominant of the two N species in glasses with the $N/P \geq 0.26$.

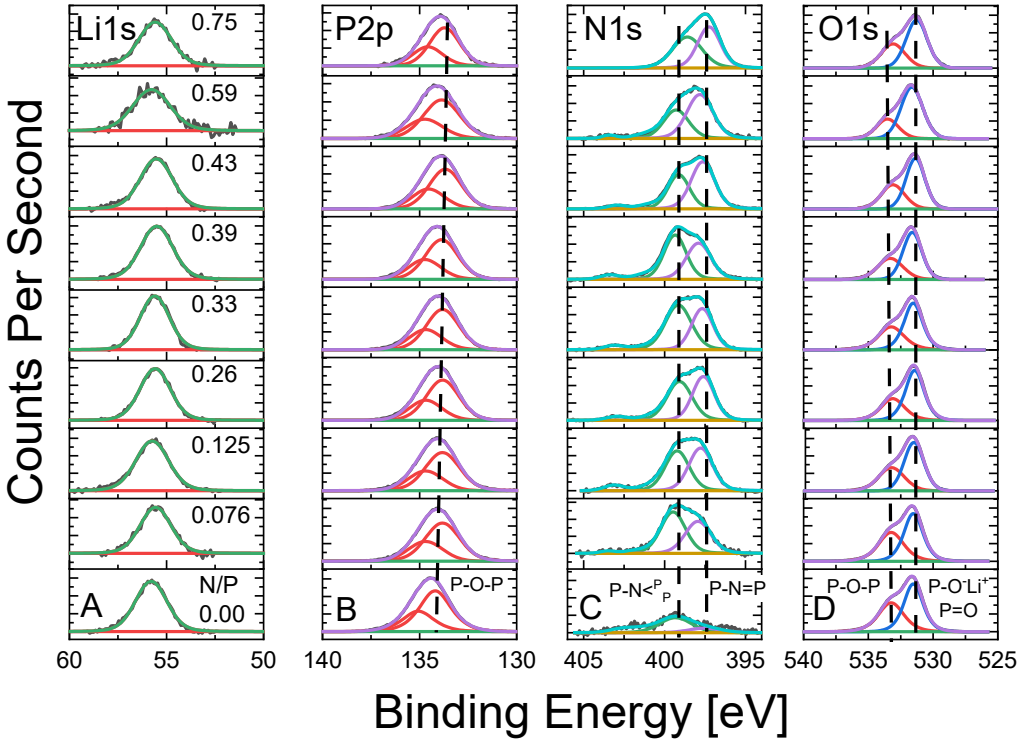

Figure 2. XPS Li1s (A), P2p (B), N1s (C), and O1s (D) spectra for LiPON glasses referenced to C1s at 286.4 eV.

The ^{31}P MAS-NMR spectra were collected on these glasses to examine the local bonding environments and quantify the various P SRO structures and species in these glasses as a function of the N/P ratio. Figure (4A) shows the ^{31}P MAS NMR spectra for the nitrided glasses from N/P = 0 to 0.75. The spectra of the un-nitrided glass shows a single strong peak arising from the expected P^2 SRO units of $LiPO_3$ at -24.4 ppm, and a very small peak arising from P^1 SRO units of $P_2O_7^{-2}$ located at -5.3 ppm.[34, 35] This latter peak presumably arises from the unavoidable but very small amount of water in these glasses arising from the decomposition reaction shown in Eq. (3) above. This residual water content acts as a chain terminator to form terminal P^1 units of the form -P(O)(OLi)(OH).[36]

As nitrogen is incorporated into the glasses, there is an observed increase in the intensity of peaks located in the region from –24 to 0 ppm along with a sharp decrease in the intensity of the P^2 resonance at -24 ppm. The minor peak at -5.3 ppm assigned to the P^1 terminal unit disappears from the spectra. These changes are a result of the formation of PO_3N^{-1} and $PO_2N_2^{-1}$ species with added nitrogen which have P MAS NMR peaks located approximately at –13 ppm and –2 ppm, respectively.[34] The structures are given in Fig. 3.

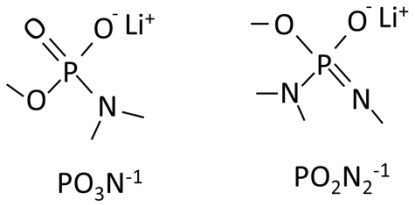

Figure 3. Chemical SRO structures of PO_3N^{-1} and $PO_2N_2^{-1}$ species.

While the chemical shifts of all of these peaks remain essentially constant for all of these glasses, the intensity and associated areas of these peaks change progressively. The intensity (and area) of the peaks associated with the pure oxide P^1 and P^2 SRO units decreasing, and the intensity (and area) of the peaks associated with PO_3N^{-1} and $PO_2N_2^{-}1$ SRO units increasing.

We have quantified these changes by spectral deconvolution and examples of this are given in Fig. (5) for glasses with N/P = 0.00, 0.33, and 0.75 for these LiPON compositions. Further deconvolution into each respective component can be found in the supplementary information for this paper. The atomic fractions of the individual P SRO species determined by this spectral deconvolution were corrected to be charge compensated using Eq. (4) and are given in Fig. (4B).

In Eq. (4), q_i is the charge on, and f_i is the atomic fraction of the four SRO P structural species observed in these glasses, P^1, P^2, PO_3N^{-1}, and $PO_2N_2^{-1}$.

$$-1 = \sum_{i=1}^{4} q_i f_i(z) \qquad \text{Eq. (4)}$$

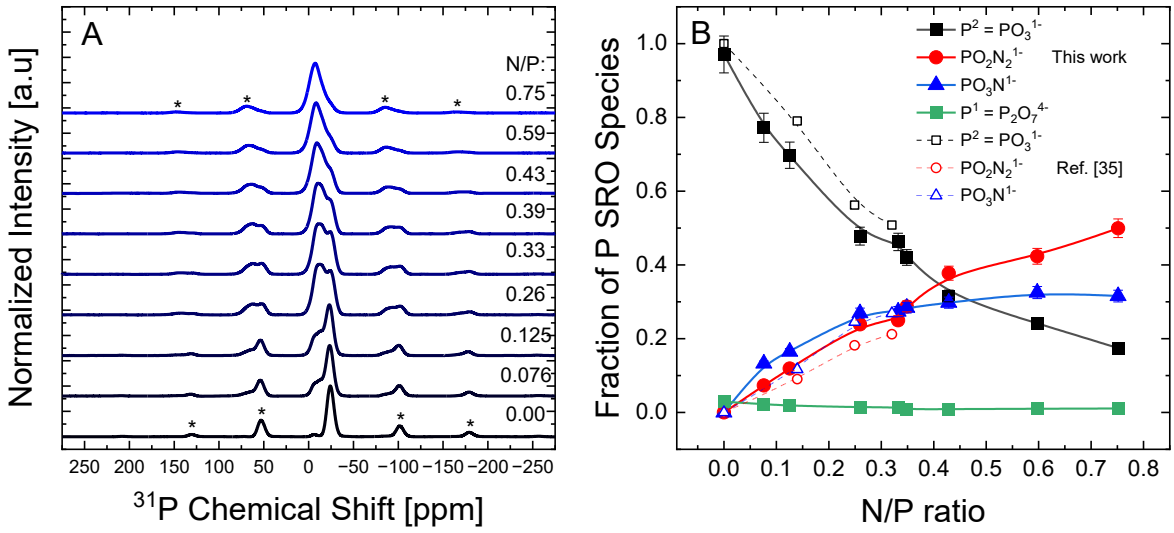

Figure 4. (A) ^{31}P NMR spectra for LiPON glasses for N/P = 0.0 to 0.75. (B) The atomic fraction, f_i of the SRO species present in these glasses as a function of N/P = z. The data from Mascaraque *et al.* [35] is shown on the graph for comparison and shows the close agreement to our work here, except Mascaraque *et al.* appear to have not included (or observed) the small amount of P^1 SRO species that we see in our glasses and only prepared and examined glasses out to z = 0.32.

As expected from the spectra, the overall trend is for the pure oxide P^2 specie to decrease in concentration and the two mixed oxy-nitride (MON) P species, PO_3N^{-1}, and $PO_2N_2^{-1}$, to increase in concentration. Similar results to ours here have been obtained by Mascaraque *et al.*, [35] but over a smaller range, $(N/P)_{max} = 0.32$, of N/P ratios than in our glasses here $(N/P)_{max} = 0.75$.

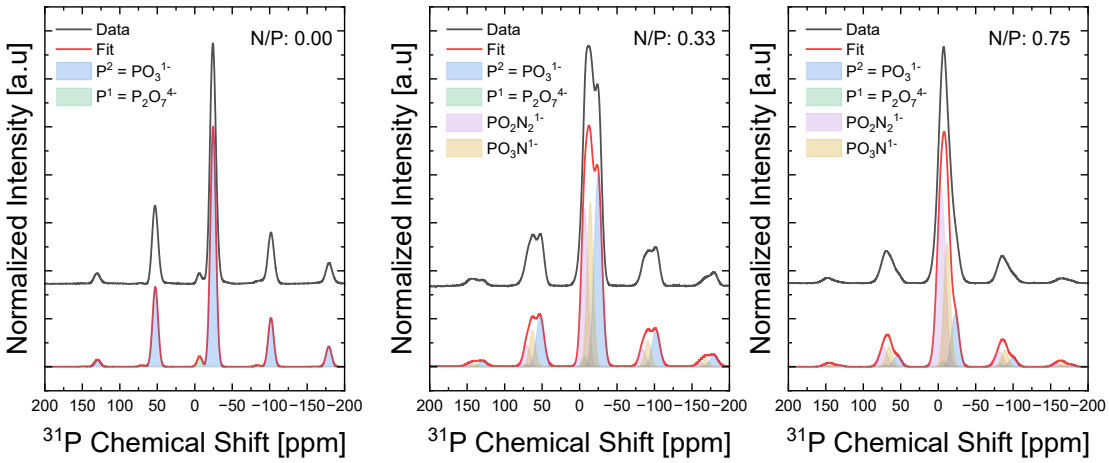

Figure 5. ^{31}P NMR deconvoluted spectra for LiPON glasses for N/P = 0.00, 0.33, and 0.75.

The results in Fig. 4(B) agree well with that of the work of Mascaraque *et al.* [35] over their smaller range of N/P ratio of 0.32. However, a very interesting change comes in at a N/P = 0.36 where the PO_3N^{-1} and $PO_2N_2^{-1}$ species overlap in roughly equal fractions, but for larger N/P ratios, the N_d SRO unit, $PO_2N_2^{-1}$, becomes the dominant species, whereas in the smaller N/P glasses, the N_t SRO unit, PO_3N^{-1}, species was the dominant PON species.

3.2 Mechanical behavior

Structural changes due to replacement of oxygen with N_t and N_d nitrogen are expected to result in changes of the mechanical properties of these LiPON GSEs. To quantify these changes, the seven different LiPON compositions with the N/P ratio ranging from zero to 0.75 were probed by depth sensing nanoindentation in CSM mode. The representative load-depth curves for the two extreme compositions are shown in Fig. 6. All of the compositions displayed strain relaxation when the load was held at 1/10th of the peak load in the unloading segment. These areas are circled in Fig. 6 (A, B). Part of this displacement can be attributed to thermal drift. It should be mentioned however that the thermal drift in these experiments was kept under 0.1 nm/s, while the calculated displacement rate from the hold periods ranges from 0.4 to 0.8 nm/s, i.e. almost ten times higher. Therefore, these displacements cannot be entirely attributed to the thermal drift and are the manifestation of time dependent relaxation in the material. Similar observations have been reported for LiPON thin films obtained via RF magnetron sputtering.[12, 13] It is interesting to note that the rate of this relaxation, calculated from the load-depth data, decreases with the increase of

nitrogen content in glass structure, as can be seen in Fig. 6(c). There is an apparent maximum in the strain restoration rate at N/P = 0.13 after which a continuous decrease is observed to the minimum value at maximum N/P = 0.75. Partial substitution of oxygen with nitrogen first enhances this behavior, indicating the ability of LiPON to display time-dependent strain restoration. The same behavior can be observed in the nitrogen-free $LiPO_3$ base glass. However, substantial nitridation changes this behavior. As will be discussed below, this is connected with material hardening upon nitridation. The evidence of such hardening is visible from comparison of maximum depth of indentation in Fig. 6(A) (no nitrogen) and Fig. 6(B) (maximum degree of nitridation).

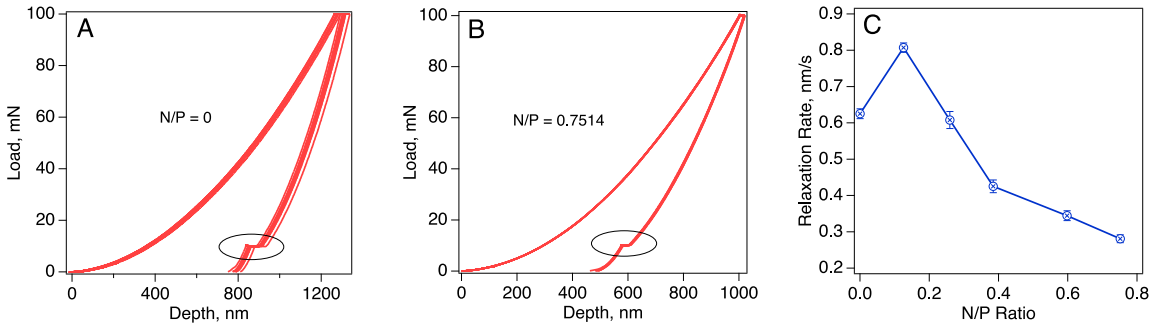

Figure 6. Nanoindentation of LiPON glasses with different degree of nitridation. (A) Load vs depth curves for nitrogen-free base glass; (B) Load vs depth curves corresponding to the maximum nitrogen content, N/P = 0.75; and (C) Strain relaxation rate as a function of glass nitridation.

The nanoindentation modulus and hardness probed as a function of indentation depth are shown in Fig. 7. Substantial instabilities at the shallow depths can be observed in some samples and are very likely due to the reacted material surface layer. The part of the data used for the modulus and hardness analysis is demarcated with the vertical dashed line in Fig. 7, indicating that the data from depths less than 300 nm was discarded. The overall trend of increasing elastic modulus and hardness with increase of nitrogen in the glass composition can be observed. This trend is further summarized in Fig. 8, where the values of the material parameters collected from nanoindentation are shown with the corresponding standard error bars. While there is significant variation in values for two of the compositions, N/P = 0.26 and N/P = 0.59, the overall trend for the hardness and elastic modulus to increase is clearly seen. A linear fit of the data is represented by dashed lines in Fig. 8 (A) and (B).

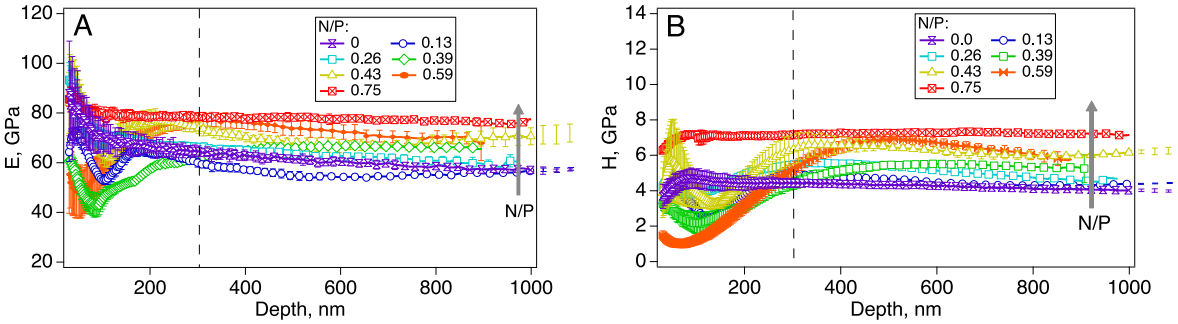

Figure 7. Modulus (A) and hardness (B) as a function of indentation depth for glasses with different composition.

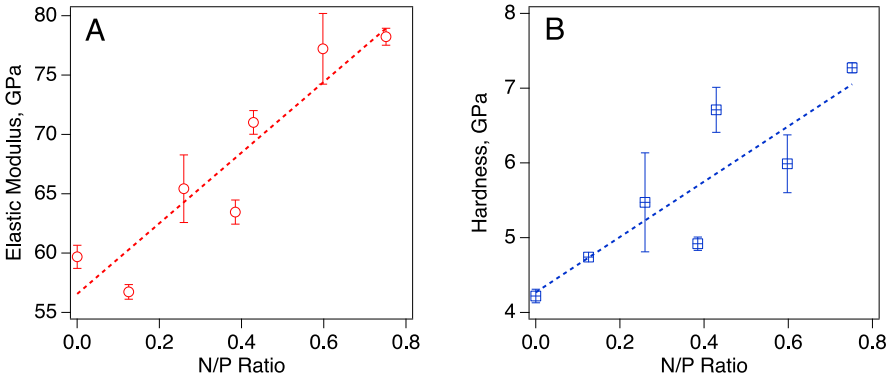

Figure 8. Variation of elastic modulus (A) and hardness (B) as a function of N/P ratio. Dashed line shows the linear fit of experimental data.

An interesting observation was made regarding the changes in resistance to fracture of LiPON glasses depending on the degree of nitridation. The increase in hardness and modulus is apparently accompanied with the loss of ductility and toughness as the nitrogen content introduced by ammonolysis increases in these glass compositions. The assessment of material brittleness at the nanoscale was performed with a sharp cube corner nanoindenter tip. The indentations were done at nominal strain rate of 0.2 s^{-1} under two maximum loads of 100 mN and 200 mN. Comparison of the residual hardness impressions in Fig. 9 clearly shows the loss of ductility in the sample with N/P = 0.75, in comparison with nitrogen-free base phosphate glass. While the nitrided sample displays radial cracks when subjected to 100 mN load, the nitrogen-free glass accommodates the same applied load without fracture. Both compositions fail under 200 mN loading, but it should be noted that in case of the $LiPO_3$ nitrogen-free composition, seven out of 36 nanoindentations did not show any cracks, while all nanoindentations triggered radial cracking in high-nitrogen glass both under 100 mN and 200 mN loads.

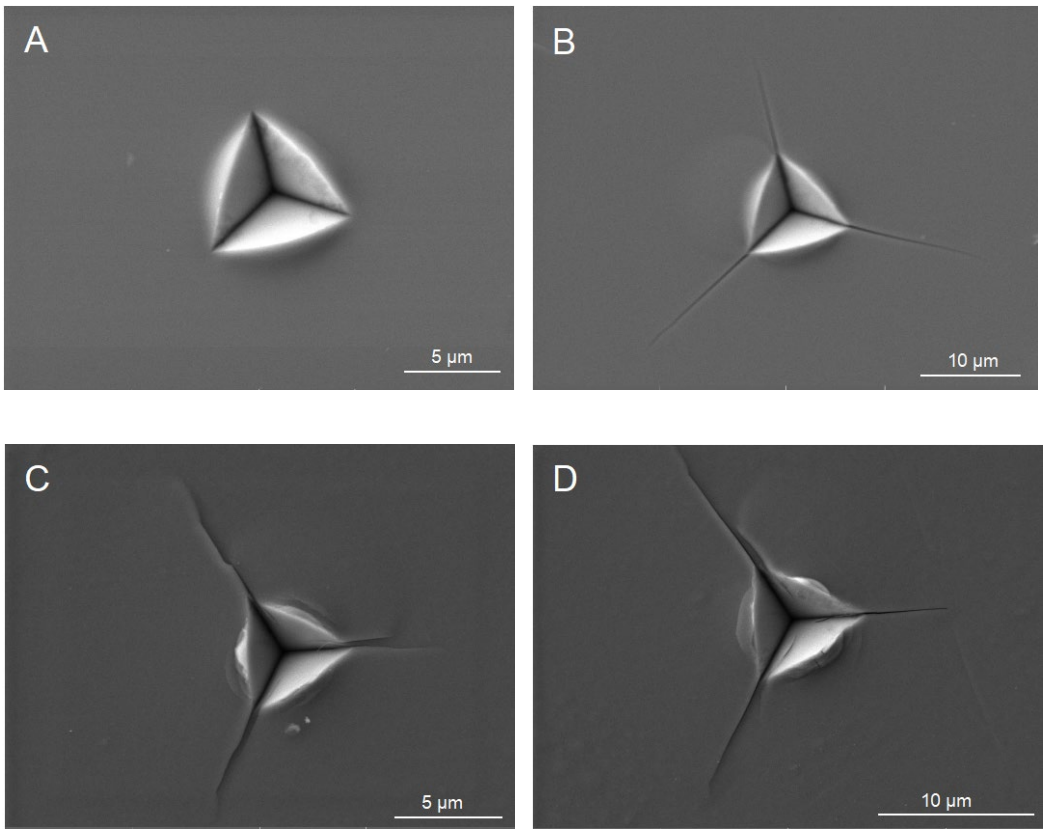

Figure 9. Nanoindentation induced residual hardness impressions and cracking patterns in (A) N/P = 0 glass under 100 mN load, (B) N/P = 0 under 200 mN, (C) N/P = 0.75 under 100 mN, and (D) N/P = 0.75 under 200 mN.

Despite cracking, the $LiPO_3$ and LiPON made by ammonolysis both display a substantial degree of pile-up around the residual hardness impressions, which is indicative of the ability to deform in shear. The presence of pile-up is evident in Figs. 9 and 10, where a side view of the residual hardness impressions is shown as recorded during in-SEM nanoindentation. The indentation in Fig. 10 shows the nitrogen-free glass indented by a cube corner nanoindenter tip with maximum applied load of 200 mN. The cracks can be seen in the central impression, as indicated by the arrows.

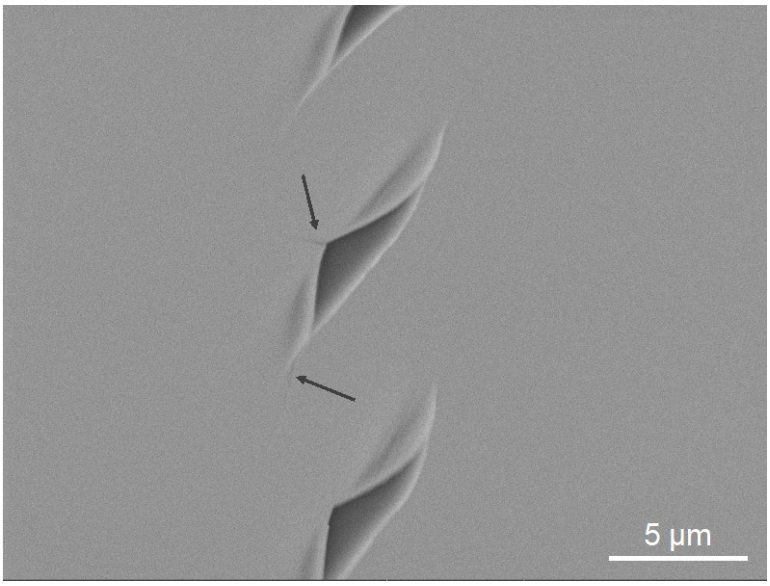

Figure 10. Small angle view of the residual hardness impressions during in-SEM nanoindentation of N/P = 0 base glass. Maximum applied load by the nanoindenter is 200 mN. Cracks are indicated by the arrows.

Plastic deformation in glasses occurs via volume conserving shear and non-conserving densification. In LiPON the latter is supported by changes in P-O-P bond angles to accommodate densification.[13] It has also been observed experimentally that such densification is partially recoverable upon removal of the applied load.[11, 13] The increase in the concentration of N_d and especially N_t nitrogen substituting oxygen at N/P > 0.4 may reduce the ability of LiPON to densify thus partially eliminating densification as a mechanism to prevent fracture.

There are two consequences of this structural change: i) increased brittleness at high nitrogen content as evident in Figs. 9 (C, D), and ii) diminished recovery of densified volume, as can be seen in Fig. 6 (C). Based on MD simulations,[13] isochoric shear in LiPON proceeds by breakage of Li-O bonds. Therefore, an ability of LiPON to deform plastically by shear depends on Li content with higher amounts of Li promoting such behavior. It should be mentioned that creating MON glasses with high alkali content by conventional melt process is extremely difficult. In this regard we should reiterate that there is a significant difference in Li content between the LiPON glass produced by ammonolysis in the current work (Li/P ~ 1), and LiPON produced by sputtering in our previous study [13] (Li/P ~ 3). The above aspects of composition can influence resistance to fracture in LiPON.

Partial nitridation of alkali metaphosphate glasses increases the network connectivity by introducing high coordinated nitrogen, N_t, atoms thus increasing the overall network rigidity. This in turn increases atomic packing density.[22] Such constriction of atomic degrees of freedom results in apparent changes of mechanical behavior at nanoscale. Both hardness and elastic modulus increase linearly with the increase of N/P ratio. The dependence of the strain reversal rate on the N/P, however, is non-linear, Fig. 6 (C). It is interesting to note, that partial nitridation up to N/P = 0.25 has been shown to increase the ionic conductivity of Li-rich (Li:P ~ 3) LiPON apparently via a decrease of the ratio of bridging to non-bridging oxygens.[26] The dual effect of nitridation is thus manifested by an increase in the ionic conductivity, but simultaneously, a decline in material ductility (increase in hardness) and toughness (resistance to fracture). However, in compositions up to N/P = 0.25, enhancement of both conductivity and mechanical properties seems achievable.

4 Conclusions

We have produced lithium phosphorus oxynitride, LiPON, bulk glasses with different contents of nitrogen by ammonolysis of $LiPO_3$ melts. The structure of glasses was characterized by Raman, FTIR, XPS, and MAS NMR spectroscopies. The structural changes due to incorporation of nitrogen were correlated with the changes in mechanical behavior of LiPON resulting in the following major observations.

- An increase in N/P ratio leads to diminished ability of LiPON to densify and to partially restore densification. The latter dependence is however non-linear.
- An increase in N/P ratio leads to an increase in both the elastic modulus and hardness of LiPON.
- LiPON experiences substantial loss of ductility at high, $z > 0.36$, nitrogen contents. However, even in the brittle regime, LiPON still exhibits noticeable pile-up during nanoindentation indicating that shear flow is still operational.
- Enhanced ability to restore deformed volume after nanoindentation, i.e. relaxation rate higher than 0.6 nm/s, can be achieved in LiPON with $N/P < 0.25$.

5 Acknowledgments

At Oak Ridge National Laboratory, this research was sponsored by the U.S. Department of Energy (DOE), Office of Energy Efficiency and Renewable Energy for the Vehicle Technologies

Office's Advanced Battery Materials Research Program (Simon Thompson, Program Manager). At Iowa State University, this research was supported in part by the National Science Foundation through grant DMR 1936913, by the ARPA-E of the Department of Energy through contract numbers DE-AR0000654 and DE-AR-0000778, and by the Vehicle Technology Office within the Department of Energy though the contract DE-EE0008852.

References

[1] Mauger A, Julien CM, Paolella, A, Armand, M, Zaghib, K. Building better batteries in the solid state: a review. Materials 2019; 12 (23): 3892

[2] Pasta, M, Armstrong, D, Brown, ZL, et al. 2020 roadmap on solid-state batteries, J Phys: Energy 2020; 2: 032008.

[3] Albertus, P, Anandan, V, Ban, CM., Balsara, N, et al. Challenges and pathways toward Li-metal based all-solid-state batteries. ACS Ener. Lett. 2021; 6(4): 1399-1404.

[4] Bachman, JC., Muy, S, Grimaud, A, et al. Inorganic solid-state electrolytes for lithium batteries: mechanisms and properties governing ion conduction, Chem. Rev. 2016; 116: 140-162.

[5] Krauskopf, T, Richter, FH, Janek, J. Physicochemical concepts of the lithium metal anode in solid-state batteries, Chem. Rev. 2020; 120(15): 7745-7794.

[6] Wolfenstine, J, Allen, JL, Sakamoto, J, Siegel, DJ, Choe, H. Mechanical behavior of Li-ion-conducting crystalline oxide-based solid electrolytes: a brief review. Ionics 2018; 24: 1271-1276.

[7] Kalnaus, S, Amin, R, Parish, C, Parejiya, A, Essehli, R, Westover, A, et al. Effect of composition on mechanical properties and conductivity the dual ion conductor $Na_{1+x}Mn_{x/2}Zr_{2-x/2}(PO_4)_3$ for solid-state batteries. ACS Appl. Ener. Mater. 2021; 4: 11684-11692.

[8] Nonemacher, JF, Arinicheva, Y, Yan, G, Finsterbusch, M, Kruger, M, Malzbender, J. Fracture toughness of single grains and polycrystalline $LiLaZrO_{12}$ electrolyte material based on a pillar splitting method. J. European Ceram. Soc. 2020; 40: 3057-3064.

[9] Liu, X, Garcia-Mendez, R, Lupini, AR, et al. Local electronic structure variation resulting in Li 'filament' formation within solid electrolytes, Nature Mater., 2021; 20: 1485-1490.

[10] Li, J, Ma, C, Chi, M, Liang, C, Dudney, NJ. Solid electrolyte: the key for high-voltage lithium batteries. Adv. Energy Mater. 2015; 5: 1401408.

[11] Herbert, EG, Dudney, NJ, Rochow, M, Thole, V, Hackney, SA.On the mechanisms of stress relaxation and intensification at the lithium/solid-state electrolyte interface. J. Mater. Res. 2019; 34: 3593-3616.

[12] Herbert, EG, Tenhaeff, WE, Dudney, NJ, Pharr, G.M. Mechanical characterization of LiPON films using nanoindentation. Thin Solid Films 2011; 520: 413-418.

[13] Kalnaus, S, Westover, AS, Kornbluth, M, Herbert, E, Dudney, NJ. Resistance to fracture in the glassy solid electrolyte Lipon. J. Mater. Res. 2021; 36(4): 787-795.

[14] Marchland, R. Nitrogen containing phosphate glasses. J. Non-Crystall. Solids 1983; 56: 173-178.

[15] De Souza, JE, De Souza, SJ, Gebhardt, R, Kmiec, S, Whale, A, Martin, SW. LiPON and NaPON glasses: A study of the ammonolysis of lithium and sodium metaphosphate melts. Int. J. Appl. Glass Science 2020; 11: 78-86.

[16] Oliver, W, Pharr, G. Measurement of hardness and elastic modulus by instrumented indentation: Advances in understanding and refinements to methodology. J. Mater. Res. 2004; 19: 3.

[17] Harding, D, Oliver, W, Pharr, G, Cracking during nanoindentation and its use in the measurement of fracture toughness. MRS Online Proceedings Library Archive 1994; 356.

[18] Zhao, R, Hu, G, Kmiec, S, Wheaton, J, Martin, SW, Torres, VW. Grain-Boundary-Free Glassy Solid Electrolytes based on Sulfide Materials: Effects of Oxygen and Nitrogen Doping on Electrochemical Performance. Batteries & Supercaps 2022; 5: e202100356.

[19] Olson, M, Kmiec, S, Martin, SW. NaPON Doping of $Na_4P_2S_7$ Glass and Its Effects on the Structure and Properties of Mixed Oxy-Sulfide-Nitride Phosphate Glass, Inorganic Chem. 2022; 61: 17469-17484.

[20] Kmiec, S, Martin, SW. Synthesis, Short-Range Order Structure, and Thermal Properties of Mixed Oxy-sulfide Nitride (MOSN) Glasses. Inorganic Chem. 2021; 60 (18): 13968-13981.

[21] Kmiec, S, Joyce, A, Bayko, D, Martin, SW. Glass formation and structure of melt quenched mixed oxy-sulfide $Na_4P_2S_{7-x}O_x$ glasses for $0 \leq x \leq 5$. J. Non-Crystalline Solids 2020; 534: 119776.

[22] Paraschiv, GL, Munoz, F, Jensen, LR, Yue, Y, Smedskjaer, MM, Impact of nitridation of metaphosphate glasses on liquid fragility. J. Non-Crystalline Solids 2016; 44: 22-28.

[23] Munoz, F, Duran, A, Pascual, L, Montagne, L, Revel, B, Rodrigues, ACM. Increased electrical conductivity of LiPON glasses produced by ammonolysis. Solid State Ionics 2008; 179(15-16): 574-579.

[24] Munoz, F, Pascual, L, Duran, A, Montagne, L, Palavit, G, Berjoan, R, Marchand, R. Structural study of phosphorus oxynitride glasses LiNaPbPON by nuclear magnetic resonance and x-ray photoelectron spectroscopy, J. Non-Cryst. Solids 2003; 324(1, 2): 142-149.

[25] Chowdari, BVR, Tan, KL, Chia, WT. Raman and X-ray photoelectron spectroscopic studies of lithium phosphotungstate glasses. Solid State Ionics 1992; 53-56: 1172-1178.

[26] Mascaraque, N, Fierro, J-L, G., Duran, A, Munoz, F. An interpretation for the increase of ionic conductivity by nitrogen incorporation in LiPON oxynitride glasses. Solid State Ionics 2013; 233: 73-79.

[27] Moreau, F, Duran, A, Munoz, F. Structure and properties of high Li_2O-containing aluminophosphate glasses. J. European Ceram. Soc. 2009; 29(10): 1895-1902.

[28] Xiao, Y, Zhong, X, Guo, J, Zhou, C, Zuo, H, Liu, Q, et al. The role of interface between LiPON solid electrolyte and electrode in inorganic monolithic electrochromic devices. Electrochim. Acta 2018; 260: 254-263.

[29] Misbah, MH, Doweidar, H. Transformation of $Li_4P_4O_{12}$ rings into $LiPO_3$ chains by CoO or CuO doping: Crystallization-induced reduction of photoluminescent Cu+ to plasmonic Cu° glass-ceramics Ceram. Int. 2021; 47 (9): 12695-12705.

[30] Le Sauze, A, Montagne, L, Palavit, G, Fayon, F, Marchand, R. X-ray photoelectron spectroscopy and nuclear magnetic resonance structural study of phosphorus oxynitride glasses, 'LiNaPON', J. Non-Cryst. Solids 2000; 263-264: 139-145.

[31] Khattak, GD, Mekki, A, Wenger, LE. X-ray photoelectron spectroscopy (XPS) and magnetic susceptibility studies of vanadium phosphate glasses. J. Non-Cryst. Solids 2009; 355 (43): 2148-2155.

[32] Mascaraque, N, Fierro, JLG, Munoz, F, Duran, A, Ito, Y, Hibi, Y, Harada, R, Kato, A, Hayashi, A, Tatsumisago, M. Thio-oxynitride phosphate glass electrolytes prepared by mechanical milling. J. Mater. Res. 2015; 30 (19): 2940-2948.

[33] Brow, RK, Reidmeyer, MR, Day, DE. Oxygen bonding in nitrided sodium- and lithium-metaphosphate glasses. J. Non-Cryst. Solids 1988; 99 (1): 178-189.

[34] Muñoz, F, Ren, J, van Wüllen, L, Zhao, T, Kirchhain, H, Rehfuß, U, Uesbeck, T. Structure and Dynamics of LiPON and NaPON Oxynitride Phosphate Glasses by Solid-State NMR. J. Phys. Chem. C 2021; 125 (7): 4077-4085.

[35] Mascaraque, N, Durán, A, Muñoz, F, Tricot, G. Structural Features of LiPON Glasses Determined by 1D and 2D ^{31}P MAS NMR. Int. J. Appl. Glass Science 2016; 7 (1): 69-79.

[36] Bunker, BC, Arnold, GW, Wilder, JA. Phosphate glass dissolution in aqueous solutions. J. Non-Cryst. Solids 1984; 64 (3): 291-316.